

Optimizing Ionic Transport in Polymer (PEO) – Garnet (LLZO) Composite Solid-State Electrolytes

*Andres Villa, Juan Carlos Verduzco and Ernesto E. Marinero**

School of Materials Engineering, Purdue University, Neil Armstrong Hall of Engineering, 701 West Stadium Avenue, West Lafayette, IN 47907

KEYWORDS: Polymer composite electrolyte, lithium ion transport, spherulite, ionic conductivity, doped LLZO, Poly(ethylene oxide), LiTFSI, microstructure, filler particles.

ABSTRACT. Polymer composite electrolytes (PCEs) are viable candidates to replace the flammable organic liquid electrolytes in current lithium-ion batteries and to exploit new electrochemistries for beyond-Li devices. The addition of fillers in PCEs has been reported to suppress the crystalline fraction in the polymer phase and increments of their ionic conductivity are ascribed to enhanced degrees of segmental motion of the amorphous phase that facilitate ion transport. However, there is evidence that ionic conductivity in semi-crystalline poly(ethylene oxide) (PEO)-based electrolytes is higher than in fully amorphous PEO electrolytes. A comprehensive mechanism for ion transport in PCEs has yet to be developed, and it is not fully understood why the weight or volume load of filler particles added to PCEs, varies widely to achieve the maximum ionic conductivity in different material systems. This work investigates

ionic transport in PCEs comprising $\text{Li}_6\text{La}_3\text{ZrBiO}_{12}$ (Bi-LLZO) and $\text{Li}_{6.25}\text{La}_3\text{Zr}_{1.25}\text{Bi}_{0.75}\text{O}_{12}$ (0.75Bi-LLZO) mesoparticles as fillers embedded in PEO: LiTFSI matrixes. The results are analyzed in terms of the composite material morphological properties. The role of the Bi content in LLZO garnet particles on the PCE ionic conductivity, the polymer phase crystallinity and the PCE microstructure are investigated. We find that the Bi content of the garnet mesoparticles determines the weight load required to achieve the highest ionic conductivity in the PCEs studied in this work. The optimum weight loads for Bi-LLZO and 0.75Bi-LLZO particle additions were found to be 5% and 10% respectively. Polarized light microscopy observations of the polymer morphology reveal significant changes in spherulite size and density as a function of garnet particle weight load. The maximum IC is observed for morphologies exhibiting large interconnected spherulites. We conclude that the density of Li vacancies, controlled by the Bi content, in the garnet crystalline structure, dominates spherulite nucleation density and growth in the polymer matrix. The optimum particle weight load results in the formation of an interconnected network of lamellar amorphous regions which is responsible for the optimum ionic conductivity. Therefore, ion transport in these composite materials requires the optimization of the Li molar ratio in the filler, and of the weight load in the PEO:LiTFSI matrix.

INTRODUCTION

Liquid electrolytes currently employed in lithium ion batteries (LIB) are flammable organic materials and concerns about their safety hinder the LIB wider implementation in critical sectors such as transportation¹. Solid state electrolytes (SSE) with high ionic conductivity (IC) across the operating temperatures of electric vehicles are of utmost interest in current battery research². Solid polymer electrolytes offer several advantages, such as flexibility and high mechanical strength, however, they exhibit low ionic conductivity at room temperature³. Adding inorganic fillers such as Al_2O_3 ⁴, MgO ⁵ and oxide garnets such as $\text{Li}_7\text{La}_3\text{Zr}_2\text{O}_{12}$ (LLZO) to PEO:salt systems⁶⁻⁸ is reported to increase their ionic conductivity. A decrease of the extent of crystallinity in the polymer matrix upon filler addition, is attributed to be responsible for the IC increment^{9,10}. The materials properties of the fillers, including particle size¹¹, surface chemistry¹² and their intrinsic ionic conductivity¹³ have been reported also to influence in ionic conductivity in PCE films. The amount of filler necessary to increase IC of PEO-based PCEs has been found to depend in addition to the nature of the filler material, on the ratio of EO:Li provided by the solvated Li-ionic salts and on the polymer molecular weight (MW). This amount has been reported for different filler materials to range from ~5wt% to ~52%wt^{4,7,8,13,14}.

The cubic phase of LLZO was first reported by Murugan *et al.*¹⁵ to exhibit ionic conductivities as high as 3×10^{-4} S/cm at 25°C, and significant efforts to further increment IC, have focused on aliovalent substitution at the Li, La and Zr sites and on sintering processes to achieve the highest ceramic pellet densification. Dong *et al.*¹⁶ synthesized $\text{Li}_{6.6}\text{La}_3\text{Zr}_{1.6}\text{Ta}_{0.4}\text{O}_{12}$ garnets and utilizing high pressure, spark plasma sintering at 1050°C, they obtained pellets with relative densities of 0.94 that exhibited an ionic conductivity of 1.18×10^{-3} S/cm at room temperature.

Solid state electrolytes based on oxide garnets excel in chemical and electrochemical stability, mechanical strength and electrochemical oxidation voltage stability; however, some of their notable disadvantages include brittleness, excessive fabrication costs and the formation of large ohmic barriers at electrode interfaces and grain boundaries. Polymer electrolytes on the other hand, offer advantages such as stability against Li-metal, flexibility and low-cost materials; however, their thermal stability, low oxidation voltages and inferior room temperature IC are severe limitations for their implementation in battery devices. A hybrid composite polymer-garnet particle solid state electrolyte can potentially combine the best attributes of the constituent materials. The fabrication of PCE membranes and thin films as discussed in this work is straightforward and it is amenable to batch production and scalable manufacturing. Furthermore, as reported in this work and by others^{7,17}, utilizing relatively low contents of filler materials, the ionic conductivity of the polymer-salt matrix can be drastically improved. As indicated in this work, with additional constituent material property improvements, the IC of PCE could potentially match that of the pure garnet ceramics. This would result in significant reductions of the rare-earth (such as La) material needed, thereby drastically reducing the electrolyte cost. Furthermore, if parity in IC between these PCEs and pure ceramic garnets can be achieved, energy intensive and costly sintering processing of the ceramic powders to form high density solids can be eliminated.

Regarding the role of the filler particle on the PCE ionic conductivity increment, we note that if the sole mechanism for the increment was on account of higher amorphous fraction induced by the fillers in the polymer matrix^{9,10}, it would be expected that an electrolyte with a maximum amorphous fraction would provide optimum ion transport. However, semi-crystalline systems have been reported to outperform fully amorphous PCE¹⁸, and several reports on IC improvements of PCEs do not correspond to the lowest degree of crystallinity in the polymer phase¹⁹⁻²¹. Recent

research in PCE has focused on increasing the ionic conductivity by engineering the morphology of the PCE to enable rapid ion transport, through the judicious choice of particle shape^{22,23}, particle alignment^{23,24}, and through constructing channels beneficial to ionic conduction²⁵. These reports indicate that IC can be significantly improved by aligning the fillers in the direction of lithium transport^{22,26}. Several methods have been explored to design ion transport efficient PCE microstructures, such as ice-templated growth of LATP²⁴, or LAGP²⁵; 3D membrane network growth of Al-doped LLZO²⁷; development of an aligned garnet framework using a wood-templated cellulose fiber structure (from basswood) for vertical alignment and incorporation of PEO to facilitate ion transport²⁸; and a method combining electro-spinning, hot-pressing and quenching to produce a LLTO 3D network in PEO²⁹. For these polymer morphology designed systems, a range of IC values ranging from $0.52 \times 10^{-4} \text{S/cm}^{24}$ to $1.8 \times 10^{-4} \text{S/cm}^{28}$ at room temperature are reported, and evidence suggests that lowering tortuosity for the Li-ion pathways improves ion transport.

In this work we provide evidence for a versatile method to optimize Li-ion transport in PCEs by controlling the polymer morphology below its melting point and for low ionic salt content, namely, through the chemical and structural manipulation of the filler garnet mesoparticles. Addition of Bi-doped LLZO particles to PEO:LiTFSI matrixes introduces charged sites on the particle surface which act as Lewis-acid base centers²¹ that enhance the kinetics of lithium salt disassociation³⁰. These surface-charged sites originate from lithium vacancy defects that are created through aliovalent substitution in LLZO by Bi at the Zr-site. We report on the influence of the Bi content in LLZO filler particles on the PCE microstructure and its ionic conductivity. Based on our observations, we propose a mechanism for enhanced Li-ion transport in these polymer-ceramic particle electrolytes.

EXPERIMENTAL SECTION

$\text{Li}_{7-x}\text{La}_3\text{Zr}_{2-x}\text{Bi}_x\text{O}_{12}$ garnet powders were synthesized using a sol-gel Pechini method described in prior publications from our group³¹⁻³⁴. The composition of the garnet powders employed in this work are $\text{Li}_{6.25}\text{La}_3\text{Zr}_{1.25}\text{Bi}_{0.75}\text{O}_{12}$ (0.75Bi-LLZO) and $\text{Li}_6\text{La}_3\text{ZrBiO}_{12}$ (Bi-LLZO). The high IC garnet cubic phase was obtained after powder calcination at 700°C for 10 hours.

To avoid deviation from nominal stoichiometry due to Li loss during calcination, an excess of 10% of LiNO_3 (99.0% Sigma Aldrich) was utilized. Bismuth doping was chosen for aliovalent substitution in LLZO garnets at the Zr-site as we³¹⁻³⁴ and others³⁵ have reported that it stabilizes the cubic phase at significantly lower calcination temperatures than for other dopants. The Bi-valence state on the of Zr^{4+} site is reported³⁵ to be Bi^{5+} . Synchrotron EXAFS studies in our previous work reveal that Bi occupies the Zr-site exclusively³³. This modifies the garnet stoichiometry and due to charge equilibration it changes the Li-site occupancy as reported by Wagner et al.³⁵ in their studies of cubic $\text{Li}_{7-x}\text{La}_3\text{Zr}_{2-x}\text{Bi}_x\text{O}_{12}$. Thus, Bi-aliovalent substitution results in an increment of Li-vacancies at the Li-site. Bi doping of LLZO lower also the sintering temperature needed for sample densification, a key requirement needed for attaining the highest IC in pure garnet ceramic solids³⁶.

Although ICP analysis was not performed in our samples to confirm the garnet's stoichiometry and Bi-content, sol-gel synthesis methods, when rigorously performed, are reported in the literature to provide accurate stoichiometry control and nominal compositions agree well with values determined by ICP. For example, Al-LLZO was synthesized using a sol-gel method with 10% mol excess Li and produced a 2.5%wt difference between nominal and experimental dopant content³⁷. In another work, Li et al.³⁸ used a sol-gel method to produce Ca-LLZO, Ba-LLZO and Sr-LLZO, again with 10% excess of Li and corroborated with ICP-OES³⁸. The difference between

nominal and experimental amount was 2.5% mol for Sr, 1% mol Ba, and no difference for Ca-doped LLZO.

The garnet powders were mixed with poly(ethylene oxide) (PEO, Sigma Aldrich, molecular weight 100,000), lithium bis(trifluoromethanesulfonyl)imide (LiTFSI, Sigma Aldrich, 99.8%) and acetonitrile (ACN, Sigma Aldrich, 99.9%) was used as solvent to mix the composite materials. ACN was mixed at a 2.5:1 liquid to solids ratio to form the PCE slurry. An EO:Li ratio of 49:1 was selected in this work based on prior studies from our group³² that determined this ratio to be the optimum value for highest IC in PCEs comprising PEO (MW=100,000) loaded with Bi-doped LLZO filler particles. The ratio in our experiments was varied from 30:1 to 98:1. PCE films made using ratios closer to the literature-reported³⁹ optimal value of PEO:LiTFSI ratio between 24 and 16 did not fully solidify. We note that in this paper they employed PEO with MWs of 1.2×10^6 and 3.9 to 5.45×10^3 , and they confirmed that IC can be correlated with the EO:Li ratio independent of MW. This is attributed to the combination of free cation-anion from LiTFSI and the presence of LLZO particles, which prevent PEO reorganization.

All the materials were mixed, and wet ball-milled for 12 hours at 400 rpm with a Fritsch Pulverisette 6 apparatus. Milling for 12 hours at 400 rpm yielded mesoparticles of ~ 437 nm (d_{50}) in size. Of potential concern is the effect of the ball milling parameters chosen in this work on the polymer chain breakdown and its effect on the PEO inherent ionic conductivity. Whereas there is evidence suggesting that ball-milling increases ionic conductivity by inducing breakdown of the PEO chain⁴⁰, we note that studies of the PEO:LiTFSI system employing PEO with MW from 10,000g/mol to 100,000g/mol, conclude that the ionic conductivity over this wide MW range does not change dramatically⁴¹. Furthermore, although changes in the PEO MW in our work due to high-energy ball milling in PEO MW are possible, all samples were prepared under identical ball-

milling conditions, as well as solvent evaporation time and temperature equilibrium time. Therefore, we expect its potential effect to be the same for all samples studied. Additional details of the effect of ball-milling parameters on garnet particle size are given in the supplementary information (Figs S1 and S2).

We also compared the effect of adding non-ionically conductive filler particles on the IC of PEO:LiTFSI with identical EO:Li ratios. To this aim, the polymer matrix was loaded with 5%wt Al₂O₃ particles (Almatis, 16-SG, d₅₀=500nm). All PCE films were prepared by pouring the slurry into molds of different depths and surface area to study the IC dependence on film thickness. All films were dried for 72 hours at room temperature in air to allow slow evaporation of ACN. Thereafter, the films were held in vacuum overnight to completely remove the solvent. Although LLZO has shown to be stable in ACN⁷, formation of lithium carbonate during processing is an ongoing concern, and determination of the presence of carbonates in the bulk or on the surface of the garnet particles has not been conducted in this work. However, the amount potentially formed and any effects that the carbonates may have on the mesoparticle properties, can be expected to be similar on all samples, as they are prepared under identical conditions and all Bi-doped LLZO used in fabricating the PCEs were obtained from the same synthesis batch. We plan to quantify the potential effect of carbonate formation by performing the synthesis of the composites under different humidity environmental conditions.

To benchmark IC values in the PCEs to those obtained in pellet ceramic samples of the same composition as the filler particles, the calcined powders were sintered at 900°C for 10h and to avoid Li volatilization during calcination, the pellets were covered in precursor powder.

Ionic conductivity was characterized using Electrochemical Impedance Spectroscopy (EIS). Temperature dependent measurements were performed at 22.5°C, 35°C, 45°C and 55°C, with a

custom-built Swagelok-type cell using two stainless steel electrodes whose separation was adjusted to maximize contact with the PCE film. Highly reproducible measurements were obtained once full contact with the films was established. Variations in IC measurements, arose mostly from temperature fluctuations during characterization, , as well as from the surface roughness of the electrode and the film itself. Therefore prior to measurements, the PCE and electrode components were allowed to reach thermal equilibrium over a 2h time period at which point, no detectable drifts were noted. The reproducibility of Nyquist plots upon repeated measurements was utilized as a criterion for optimum contact. Following this procedure enabled us to determine IC values within $\pm 10\%$ reproducibility for all samples and temperatures studied. A Solartron SI 1260 impedance/gain-phase analyzer and SI 1287 electrochemical interface operating in the frequency range 100mHz to 300kHz was employed. An AC potential of 50mV was applied to the PCE membrane. Representative examples of Nyquist plots are presented in the supplementary information (figure S5) together with a description of the methodology employed to extract IC values. The cubic nature of the LLZO garnet was verified by XRD employing a Bruker D-8 Focus apparatus, Cu source (1.54\AA), using a scan rate of $5^\circ/\text{min}$. The microstructure of the PCE films was investigated with XRD using a scan rate of $2.5^\circ/\text{min}$, as well as with FTIR and SEM. Polarized light microscopy (PLM) was employed to investigate spherulite formation as a function of LLZO particle weight load.

RESULTS AND DISCUSSION

Fig. 1(a) presents the XRD scan for the 0.75Bi-LLZO powder sample, whereas Fig. 1(b) corresponds to that for Bi-LLZO. In Fig. 1(c) the reference pattern for cubic LLZO is provided for comparison (ICSD collection code 185540). The cubic phase formation is verified at a calcination temperature of 700°C . Note that the peak at 28.45° is identified to correspond to $\text{La}_2\text{Zr}_2\text{O}_7$, a

common byproduct in LLZO synthesis. It has been reported that Li_2CO_3 reacts with $\text{La}_2\text{Zr}_2\text{O}_7$ to form LLZO⁴². As there are no detectable traces of Li_2CO_3 in the XRD scans shown in Fig 1, it is reasonable to conclude that not appreciably loss of Li occurs in the reaction to form of Li_2CO_3 and Li_2O . Rietveld analysis was used to estimate the amount of $\text{La}_2\text{Zr}_2\text{O}_7$ phase present in the garnet powders. For the case of Bi-LLZO the crystalline $\text{La}_2\text{Zr}_2\text{O}_7$ phase was estimated at $\sim 2.08\%$ wt, while for the 0.75Bi-LLZO powders it is estimated at $\sim 1.03\%$ wt. Details of the Rietveld analysis are provided in Fig. S7.

To assess the potential advantages regarding garnet material utilization of PCEs over pure ceramic electrolytes, we compared IC values measured in the PCEs vs. those obtained in garnet ceramic pellets of the same composition as the fillers. Measurements at 27°C of IC in pellet disks (10mm diameter, 1mm thick) fabricated by sintering the calcined powders at 900°C for 10h, were determined as $2 \times 10^{-4} \text{S/cm}$ and $1.2 \times 10^{-5} \text{S/cm}$ for 0.75Bi-LLZO and Bi-LLZO respectively.

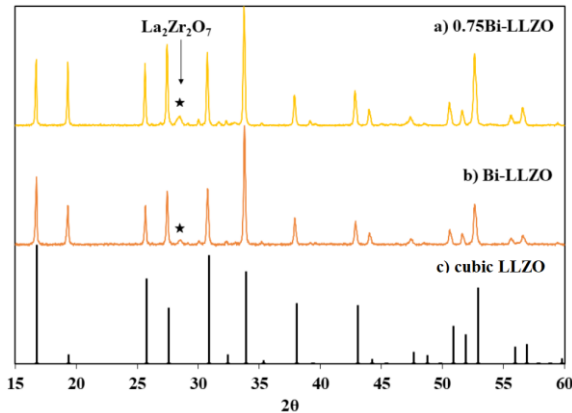


Figure 1. XRD pattern for: (a) 0.75Bi-LLZO and (b) Bi-LLZO, (c) reference PDF pattern corresponding to the cubic phase of LLZO (ICSD collection code 185540).

Whereas these values are lower than the highest reported ones for aliovalently substituted garnets¹⁶, we note that the relative density of our samples was only ~ 0.84 and densification is critical in attaining the maximum IC in pellet samples. For example, Wang and Sakamoto³⁶

reported a value of 1.0×10^{-4} S/cm in a Bi-LLZO sample having a relative density of 0.94. This is an order of magnitude higher than that measured in our sample of the same composition but lower relative density of 0.84.

Fig. 2 provides Arrhenius plots of ionic conductivity of the PCEs studied in this work as a function of particle wt% load (5%, 10%, 30%, 50%). Figs. 2(a) and 2(c) compare IC values for filler-free PEO:LiTFSI membranes with values measured when Bi-LLZO and 0.75Bi-LLZO garnet mesoparticles are added. In Fig. 2(b) the Arrhenius plots correspond to filler-free PEO:LiTFSI, and upon additions of 5%wt Al_2O_3 particles of comparable size, 5%wt Bi-LLZO and 10%wt 0.75Bi-LLZO garnet particles. The results of Fig. 2(a) and 2(c) show that the highest ionic conductivity is attained for %wt load additions of 5% and 10% for Bi-LLZO and 0.75Bi-LLZO garnet particle respectively. Furthermore, it is evident from examination of Fig. 2(b) that 5%wt load Al_2O_3 particle additions to the polymer-salt matrix does not increment its ionic conductivity. As observed in Fig. 2(c), the ionic conductivity of the filler-free matrix and with 5%wt load of 0.75Bi-LLZO exhibits virtually the same response across the temperature range studied. In contrast, when the load is increased to 10%wt, the IC is enhanced by $\sim 10x$ and $15x$ over the unloaded sample at 22.5°C and 45°C , respectively. For the case of Bi-LLZO particle addition, as observed in Fig. 2(a), the addition of both 2.5% wt load of Bi-LLZO particles drastically increments the IC of the PEO:LiTFSI matrix. The highest values of IC below 55°C , in this case correspond to additions of 5%wt loads of Bi-LLZO particles. As shown in Fig. 2(b) loading the PCE with 5%wt load of Bi-LLZO particles increases the ionic conductivity of the PEO:LiTFSI matrix by more than an order of magnitude at 22.5°C and the IC values at 22.5°C and 55°C are 2×10^{-5} S/cm and 5.45×10^{-3} S/cm at respectively. We note that PCEs loaded with 5% wt of Bi-

LLZO particles exhibit at 22.5°C higher than that of ceramic pellet of the same composition measured and 27°C (1.2×10^{-5} S/cm).

To facilitate conversion between commonly employed units for particle loading, Table 1 provides the amount of mesoparticles in these experiments in both % weight load and volume fraction. Note also that the relative densities for the Bi-LLZO and 0.75Bi-LLZO garnet materials using the Archimedes method were determined to be 0.84 and 0.83 respectively³⁴.

Table 1. Conversion from % weight load (% wt) to % volume fraction (% vf) for Bi-LLZO and 0.75Bi-LLZO particle addition to PEO:LiTFSI membranes.

	Bi-LLZO	0.75Bi-LLZO
2.5% wt	0.66% vol	0.67% vol
5% wt	1.33% vol	1.36% vol
10% wt	2.74% vol	2.8% vol
30% wt	9.86% vol	10.05% vol
50% wt	20.31% vol	20.65% vol

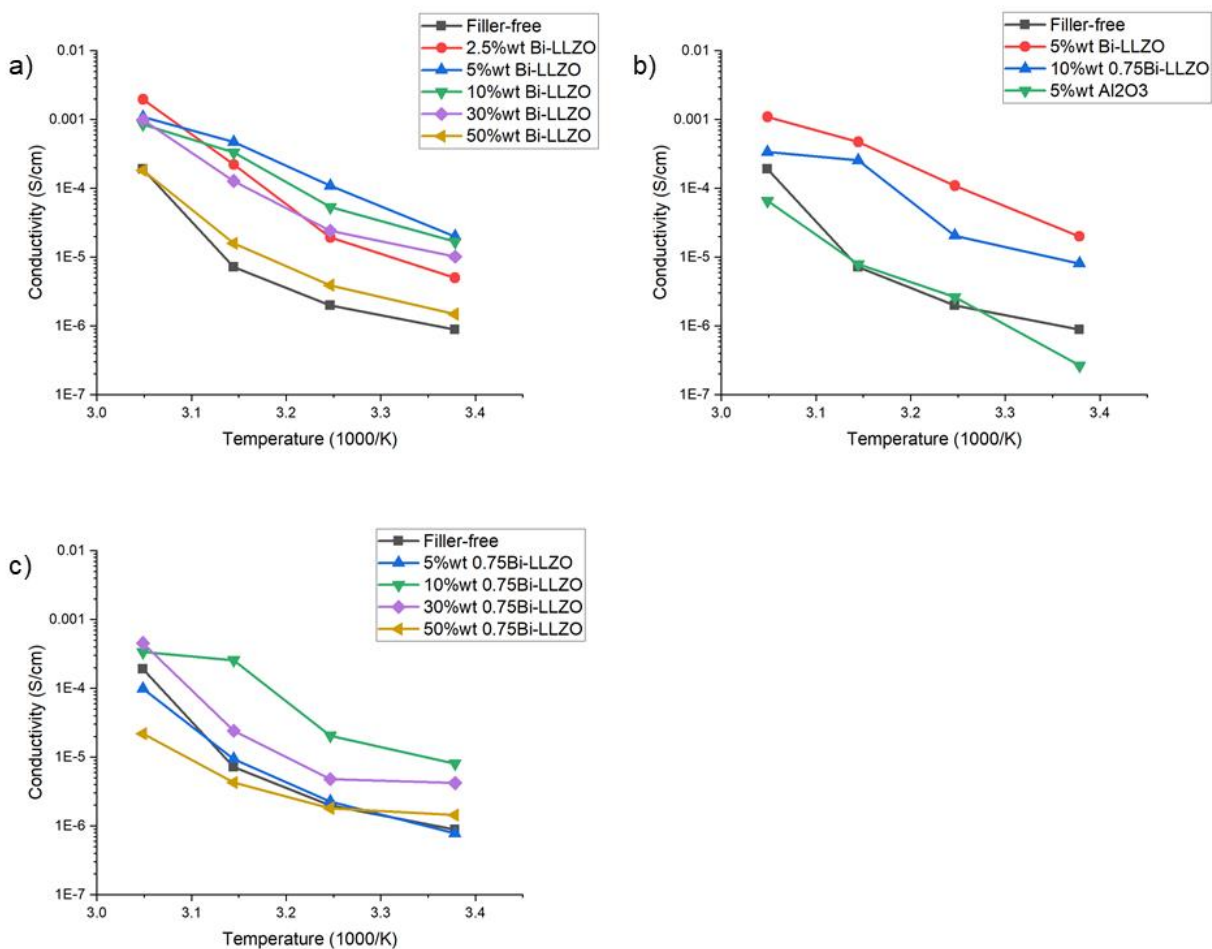


Figure 2. Temperature dependence of the IC of PCEs with different weight loads for different fillers. (a) Comparison between PCEs for active fillers based on doped LLZO, inactive filler Al₂O₃ and no addition of ceramic fillers. (b) Comparison between PCEs with filler Bi-LLZO. (c) Comparison between PCEs with filler 0.75Bi-LLZO.

Examination of the results presented in Fig. 2 provides evidence to the following important observations: 1) the amounts of particles needed to significantly improve the IC of the polymer matrix is 10%wt or lower, we note that this is significantly smaller than the particle percolation threshold. The garnet particles in the polymer matrix, as seen in Fig. S3(a) of the supplementary information, are widely separated and are homogeneously distributed; 2) the strong influence of

the garnet particles Bi-composition on the weight load amount needed to achieve the highest IC in the PCE; 3) the difference in the garnet particle stoichiometry for achieving the highest IC in the PCE and pellet samples. Our studies of the IC dependence of LLZO garnets pellets on Bi content, reveals a maximum value for Bi=0.75 and is a factor of ~17x higher than that for Bi=1.0 and 4) the IC enhancement provided by the added filler particles to the polymer matrix persists over the temperature range studied.

These observations provide evidence that the enhancement of the IC in these PCE brought about by the garnet particle additions, is not due simply to higher ionic transport within the filler particles (the particles are too widely dispersed and not interconnected) but rather, that the particle composition exerts a critical influence in the macroscopic ion transport across the polymer matrix.

Furthermore, the effect of the optimum particle load and Bi-content dependence on IC enhancement over the temperature range studied shows a similar trend. These observations are later discussed in conjunction with additional structural characterization of the PCEs in order to propose a plausible model for the enhanced transport observed in these materials.

Next, we examine the effect of the garnet particle Bi-content on macroscopic transport in the polymer matrix. The Li⁺ ion motion requires, amongst other, surmounting the energy that binds the small Li cations to the ether-bonds of the polymer chain. Collectively, mechanisms hindering ion migration can be considered as energy barriers to ion transport. The data presented in Fig. 2 is utilized to derive activation energies (E_A) from Arrhenius plots for the various particle % wt loads.

E_A is calculated from the equation $\sigma = Ae^{\frac{-E_A}{kT}}$, where σ is the ionic conductivity, A is the frequency factor, k is Boltzmann's constant and T is the temperature. The effect of adding 5% wt Bi-LLZO and 10% wt 0.75Bi-LLZO particles to the polymer matrix resulted in a decrement of E_A from 1.34eV to 1.07eV and 1.08eV respectively. E_A incremented to ~1.2 eV when 30%wt garnet

particles were added. These changes in the magnitude of E_A broadly correlate with observed changes in IC for the PCEs. Arrhenius plots for the ionic conductivities and details of the calculations are given in the supplemental information (Figs. S6 and Table S2).

To investigate the effect of garnet particle additions on the degree of crystallinity of the polymer matrix and in particular, whether the IC enhancements at the %wt observed corresponded to a significant increase in amorphous fraction, the PCE samples were characterized by XRD. Malathi *et al.*, based on XRD observed a drastic crystalline to amorphous transition when loading PEO with 5%wt powders of alumina, barium titanate and lead zirconium titanate⁴³. In contrast to their work, the results presented in Figs. 3(a) and 3(b), corresponding to XRD scans for PCE films with different %wt loads of 0.75Bi-LLZO and Bi-LLZO respectively, do not provide evidence for a crystalline to amorphous phase transition at the optimum particle %wt load consistent with the highest IC of the PCE. The peaks in the 19°- 23.5° correspond to crystalline PEO. The intensity of the peak at 23.5° is observed to decrease in intensity as the garnet particle %wt is augmented, suggestive of an increasing amorphous fraction in the polymer. However, the intensity decrement is proportional to the amount of filler particles added. It is interesting to compare the change in peak intensity when adding 5%wt Al₂O₃ vs. garnet particles: no significant change is observed for the case of Al₂O₃ and 0.75Bi-LLZO particle addition, whereas for the case of Bi-LLZO, the peak intensity decreases almost by a factor of two. The scans show also the reflections corresponding to cubic LLZO, whose peak intensities grow as the %wt of filler particles is incremented. To facilitate their identification, the reference pattern for cubic LLZO is provided. The absence of peaks corresponding to the LiTFSI salt indicates the full dissolution of the lithium salt in PEO. Hence, this XRD study does not provide evidence for significant amorphization of the polymer

matrix at the critical particle %wt observed to result in optimum IC. This is consistent with published results^{17,44}.

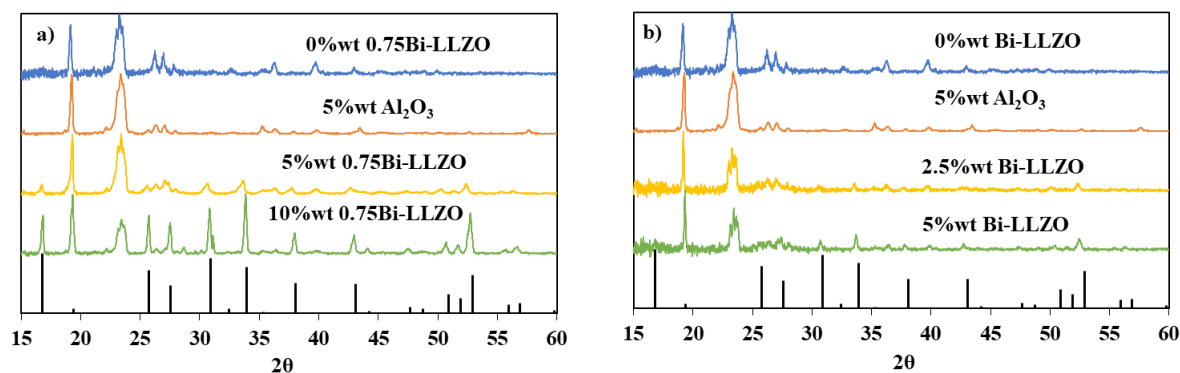


Figure 3. XRD patterns for PEO:LiTFSI with

varying weight loads of (a) 0.75Bi-LLZO and (b) Bi-LLZO. The pattern for 5% wt Al_2O_3 particle addition is also shown. For reference, the PDF pattern corresponding to cubic LLZO (ICSD collection code 185540) is displayed.

To further investigate the relationship between small changes in crystallinity and ionic conductivity, DSC measurements were performed. Fig. S4 (supplementary information) shows the DSC curves for PEO:LiTFSI films loaded with Bi-LLZO mesoparticles. Melting points were determined using the endotherm peaks between 50°C and 60°C upon heating. Melting temperature for all films are approximately 57°C, with only a small decrease in melting temperature from 57.87°C for the unloaded film compared to 57.3°C for the 5%wt Bi-LLZO film. Regarding the enthalpy of fusion, there is also very little variation with particle wt load, with a decrease from 107 J/g for the unloaded sample, compared to 104 J/g for the sample with 5%wt Bi-LLZO corresponding to the highest IC. However, the heat of enthalpy decreased for all samples with added Bi-LLZO (see Table S1 in supplementary information) to approximately the same value.

Consistent with XRD results shown in Fig. 3, only small changes in crystallinity are observed from DSC measurements. Thus, since not appreciable changes in crystallinity are observed, and IC changes dramatically for the optimal %wt load, other explanations must be considered.

To further study the effect of temperature on the PCE ionic conductivity, Fig. 4(a) presents the IC dependence for Bi-LLZO %wt additions. As expected, the IC of the unloaded PEO:LiTFSI samples increments as the temperature is raised on account of the higher vibrational excitations of the polymer molecules that lower the activation energy for ion transport. The IC enhancement induced by 5%wt Bi-LLZO addition is not constant across the temperature range studied: these are: 12x, 19x, 20x and 9x at 22.5°C, 35°C, 45°C and 55°C respectively. The increment is less pronounced at 55°C and this is attributed to the approximation of the PEO melting point (66°C - 75°C), which is lowered by the added LiTFSI salt⁴⁵. These results indicate that whereas the polymer chain molecular motions contribute to ion transport, the effect of the garnet filler particle exerts a stronger influence on incrementing IC in these PCEs. Further evidence on the effect of the particle Bi-content on IC and temperature behavior is provided in Fig. 4(b) wherein a comparison is made of the %wt dependence for 0.75Bi-LLZO and Bi-LLZO additions to PEO:LiTFSI at 22.5°C and 45°C. In addition to the difference in the %wt required to achieve the highest IC discussed earlier, it is seen that the IC enhancement persists across the range of particle additions studied.

As mentioned earlier, a wide range of filler weight loads have been reported to be needed to significantly increase IC in composite polymer electrolytes. In a recent publication, Chen *et al.*⁴⁶, report on the effect of adding Ta-LLZO garnet particles to PEO:LiTFSI from 10%wt to 80%wt. These authors indicate that with increasing concentration of fillers, different pathways for ionic transport need to be considered ranging from intrachain diffusion with interchain hopping in

“ceramic-in-polymer” systems, all the way to percolation through the filler in “polymer-in-ceramic” electrolytes.

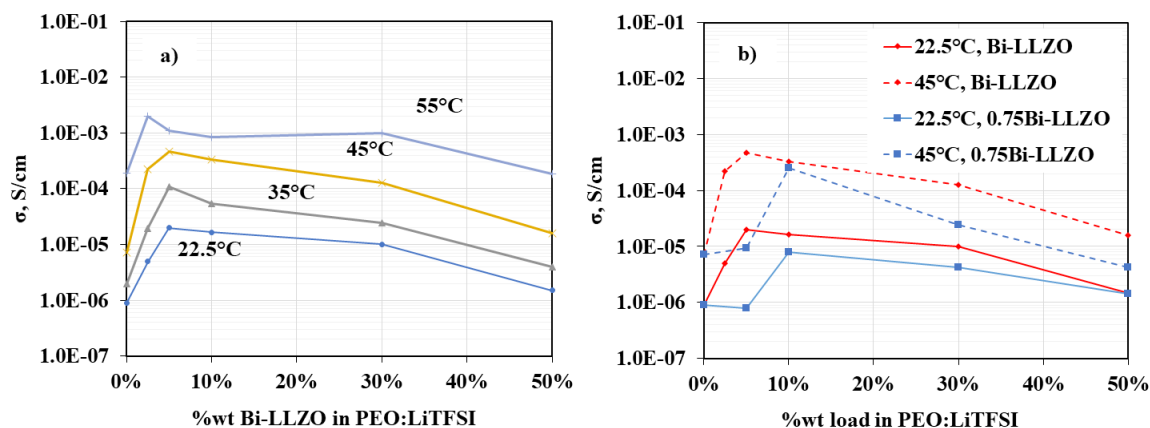


Figure 4. Ionic conductivity of the PEO:LiTFSI as a function of (a) weight load of Bi-LLZO at different temperatures; (b) IC weight load dependence at 22.5°C and 45°C for 0.75Bi-LLZO and Bi-LLZO additions.

At lower values of filler contents, the IC increment is attributed to the inorganic ceramics increasing the free volume for PEO chain segmental motions. However, the influence on the polymer morphology on the chemical composition of the filler particles on the optimum volume fraction needed to obtain the highest IC, as reported in this work, cannot be explained by this simple picture. Therefore, other factors must be considered in elucidating the transport mechanism that improve Li-ion transport in these PCEs. In particular, the influence of the physico-chemical properties of the Bi-doped LLZO fillers on the morphology of the polymer matrix.

The morphology of polymer materials and the degree of crystallinity is determined to a large extent by spherulite formation. Their formation is associated with crystallization of polymers from the melt and is controlled by the number and type of nucleation sites, the structure and chemical composition of the polymer molecules and the cooling rate from the melt. Spherulites grow radially

from nucleation centers and their growth is controlled by the polymer crystal growth kinetics and the volume competition driven by the density of nucleation sites and the dimensions of the material. Marzantowicz *et al.*⁴⁵ report on the role of spherulite formation on IC for PEO:LiTFSI of two compositions (EO:Li = 50:1 and 6:1). It is concluded that the drastic decrease of conductivity for the EO:Li=6:1 sample during crystallization is related to the closing of amorphous conductivity pathways by growing spherulites. Xi *et al.*^{47,48} have studied utilizing polarized optical microscopy and DSC the effect of incorporating ZSM-5 molecular sieves on the crystallization kinetics of PEO and shown that adding fillers to PEO has great influence on the heterogeneous nucleation and growth of spherulites in the polymer matrix.

We attempted to measure the surface charge of the garnet particles embedded in the polymer matrix and near its surface using Kelvin probe AFM and scanning electrochemical cell microscopy. Sample roughness and thickness prevented us from obtaining conclusive results. However, it has been reported that when LLZO particles are added to PEO:LiTFSI, charged sites on the particle surface act as Lewis-acid base centers²¹, that influence the kinetics of lithium salt disassociation³⁰. These surface-charged sites originate from lithium vacancy defects that are created through aliovalent substitution in LLZO with elements such as Bi, Al and Ta²¹. The role of the particle surface has been investigated with other fillers as well, such as super-acid ZrO₂⁴⁹. And mesoporous silica, alumina and titania⁵⁰.

To investigate the role of Bi-doped particle additions on the PEO:LiTFSI morphology, we employed polarized light microscopy (PLM) to study spherulite formation as a function of garnet particle %wt. Fig. 5 presents two sets of PLM images for PCE samples loaded with 5%wt and 10%wt Bi-LLZO and 0.75Bi-LLZO particles measured at 35°C. Additional details on these measurements are provided in the supplementary information. The corresponding IC dependence

on particle weight load at 35°C is also given in the figure. Average spherulite size is estimated from the PLM images for the polymer-salt matrix loaded with 5%wt and 10%wt Bi-LLZO and 0.75Bi-LLZO. This is done by examining the images under higher magnification to determine individual spherulite boundaries. The white lines in the images delineate said boundaries. From this analysis we infer that the average spherulite size for the case of the PCE loaded with Bi-LLZO particles decreased from $\sim 98\mu\text{m}$ in diameter to $\sim 39\mu\text{m}$ when the %wt was increased from 5% to 10%. Whereas for the samples loaded with 0.75Bi-LLZO particles, the spherulite average size increased from $\sim 87\mu\text{m}$ to $\sim 119\mu\text{m}$ when the %wt incremented from 5% to 10%. The corresponding IC changes are from $1.09 \times 10^{-4} \text{S/cm}$ to $5.33 \times 10^{-5} \text{S/cm}$ and from $2.27 \times 10^{-6} \text{S/cm}$ to $2.05 \times 10^{-5} \text{S/cm}$ upon incrementing the particle load from 5% wt to 10% wt for Bi-LLZO and 0.75Bi-LLZO particles respectively. The changes in spherulite size evident from the PLM images of Fig. 5 indicate that Bi-LLZO and 0.75Bi-LLZO particles are spherulite heterogeneous nucleation centers in the polymer matrix.

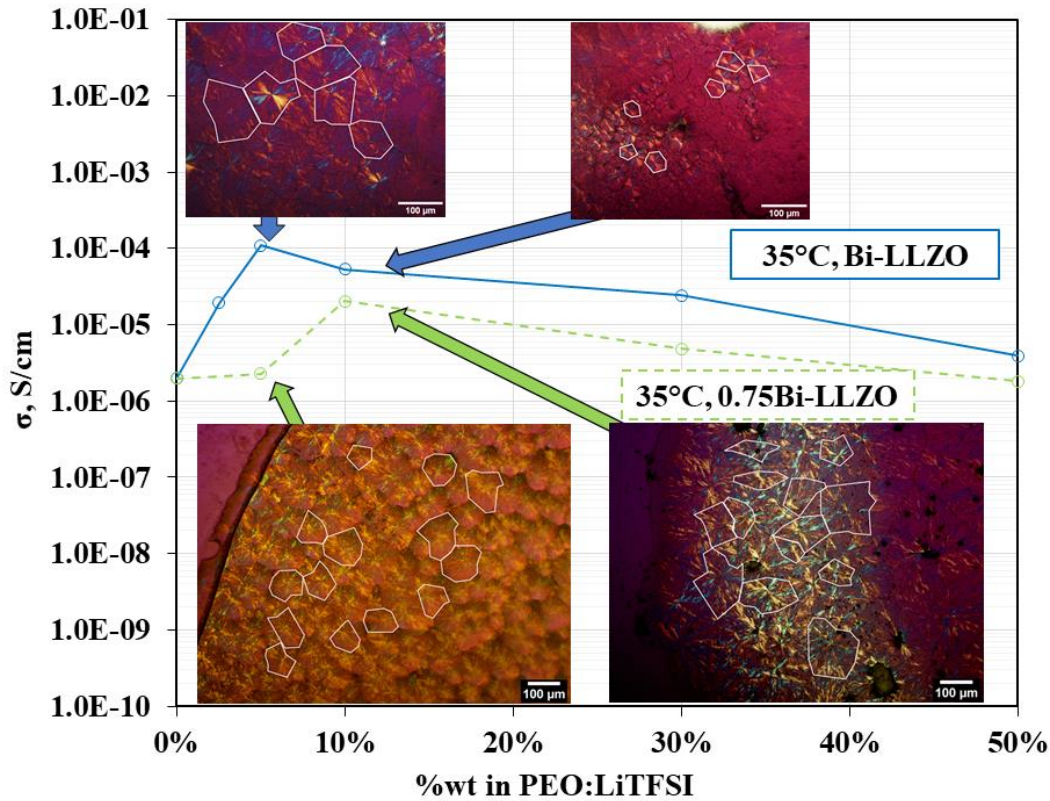


Figure 5. Ionic conductivity measurements at 35°C of PEO:LiTFSI with added Bi-LLZO and 0.75Bi-LLZO as a function of weight load. The inset images are PLM photographs of spherulites at specific weight load amounts of the filler particles. White lines delineating the spherulite boundaries are added for clarity.

To understand the relationship between spherulite formation and ionic conductivity, we first consider how spherulite formation can aid or hinder ionic conductivity in polymer matrixes. Spherulites grow radially from nucleation centers and their growth is controlled by kinetic processes in the polymer and by volume competition between multiple spherulites randomly and heterogeneously nucleated within the volume of the material. Spherulites comprise highly ordered (crystalline) lamellae connected by amorphous regions and their size can range from micrometers to millimeters. Therefore, ion transport within spherulites is anisotropic and it is expected to be

more efficient through the amorphous regions of the spherulites. At the boundary regions between spherulites, the crystalline lamellae and the amorphous regions can interconnect to either facilitate long range transport, when amorphous regions interconnect, or impede transport when the lamellae at the boundaries interconnect with amorphous regions. The most favorable situation for long range efficient ion transport results from large spherulites whose amorphous regions interconnect at the boundaries to provide interconnected transport channels. This description helps to understand the %wt load dependence on IC observed in this work: when the weight load is too small, the density of heterogeneous nucleation centers is too low and results in the formation of isolated spherulites with no interconnectivity. Conversely when the %wt of filler particles is too high, a large number of spherulites are nucleated and volume competition for growth results in the formation of numerous small spherulites. Thereby introducing a large density of spherulite boundaries which increment the ion path tortuosity and transport across ion-resistive channels involving crystalline to amorphous pathways. The optimum IC ensues when the weight load of fillers provides a critical density of heterogeneous nucleation centers that allows the formation of large spherulites which interconnect through a minimum of spherulite boundaries. This effectively reduces deleterious crystalline to amorphous inter-spherulite connections and increases the probability of formation of interconnected amorphous regions between spherulites, thereby connecting the high ionic conductivity polymer pathways and reducing ion migration tortuosity. This description is consistent with observations by Cheng et al⁵¹ and Fullerton et al⁵² regarding ion transport in polymer electrolytes.

We next consider the role of the disassociated Li from the LiTFSI salts in this system. The salt increases the charge carrier density and therefore IC. However, the presence of the ionic salt is reported to decrease the spherulite growth rate upon the polymer solidification from the melt⁴⁵.

This salt-induced decrement of spherulite growth is compensated in the PCEs by the addition of Bi-LLZO particles which act as heterogeneous nucleation sites in the polymer matrix. Based on the particle %wt influence on spherulite formation and growth observed, we conclude that the Bi-doped garnet sites dominate the overall nucleation and growth of spherulites in these PCEs. This is consistent with published studies on the effect of additives to nanocomposite materials^{53,54}. Judicious balancing of the amount of free lithium ions provided by LiTFSI disassociation, and of the added Bi-doped LLZO particles, provides an avenue to control the film morphology for optimum ion transport.

The other remarkable fact reported in this study is the influence of the Bi content in the garnet particles in determining the %wt load required for optimizing the polymer matrix IC. As discussed, additions of Bi-LLZO and 0.75Bi-LLZO require different particle %wt: 5% and 10% respectively. Furthermore, for the same EO:Li ratio and PEO molecular weight, Bi-LLZO provides a higher enhancement of IC of the polymer-salt matrix over 0.75Bi-LLZO. This last observation is evidence that the intrinsic ionic conductivity in the garnet particle alone is not the reason for the IC enhancement of the composite materials reported here. Our study of the IC dependence on Bi-content in LLZO pellets shows that 0.75Bi-LLZO samples exhibit the highest intrinsic ionic conductivities and are almost one order of magnitude higher than that measured for the Bi-LLZO specimens^{33,34}. For the case of the PCE, *the highest IC is derived when adding the lower intrinsic IC garnet particles*. Incrementing the Bi content from 0.75 to 1.0 increments the density of Li vacancies in the garnet structure while reducing the Li occupancy. We suggest that the higher density of Li vacancies alters the particle surface charges⁸ and its chemistry and this surface modifications result in three significant consequences: 1) it changes the polymer ether oxygen coordination with the Li-salt, enhancing the rate of Li-ion disassociation in a similar fashion as

lithium salt cations⁵⁵; 2) it alters the free volume for PEO chain segmental motion and 3) it changes the rate of nucleation and growth of spherulites in the polymer matrix effected by the added garnet particles. A corollary of the later observation is that a higher density of Li vacancies in the filler particle accelerates spherulite growth and the probability of forming interconnected high ion transport amorphous channels, consistent with our observations, whereby Bi-LLZO (Li-site occupancy=6.0) provides both higher IC and a lower %wt is needed to optimize the PCE ionic conductivity.

We next propose a plausible mechanism that could explain the enhancement in ionic conductivity and its dependence on particle chemistry and weight load. To this end, we use the the graphic representations given in Fig. 6 that conceptually depicts the differences in nucleation and growth of spherulites in the absence and presence of filler particles. It is emphasized that the drawings do not reflect experimental results from our work. The top panel provides a representation or the time evolution of spherulite nucleation and growth resulting from random centers formed upon PEO:LiTFSI solidification from the melt, as observed in a low salt environment¹⁸. The middle panel aims to illustrate competition for spherulite nucleation and growth from random sites and from Bi-doped LLZO particles for a subcritical amount of filler particles, whereas the lower panel illustrates the formation of a network of interconnected spherulites with optimum size and nucleated by the garnet filler particles. This illustration helps also to understand the effect of the filler particle surface charge and chemistry on IC enhancements. To begin with, when the spherulite formation is solely driven by random nucleation centers, the presence of the Li-salt as reported by Marzantowicz *et al.*⁴⁵ slows down the spherulite growth rate. Addition of garnet particles, as discussed, results in enhanced Li-salt disassociation and a faster spherulite growth rate. This accelerates the formation of interconnected, higher conductivity

regions in the polymer matrix. In the middle panel the density of heterogenous nucleation centers (garnet particle %wt) is insufficient to interconnect spherulites nucleated by the particles. Finally, the lower panel provides the optimum situation for enhanced ion transport due to the formation of an optimized interconnected polymer morphology. Moreover, as evidenced in this work, *the formation of the optimum morphology and the amount of filler required is controlled by the density of Li vacancies in the garnet crystalline structure.*

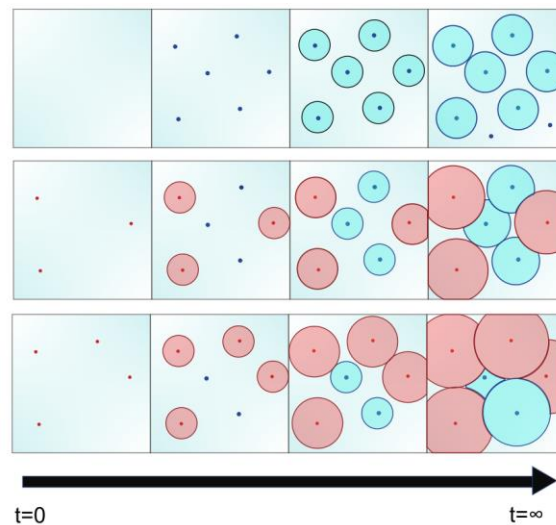


Figure 6. Pictorial representation of the formation of the optimum polymer morphology conducive to enhance ion transport. The different panels illustrate time evolution of the nucleation and growth of spherulites nucleated by random centers formed upon the polymer solidification from the melt (top panel, blue dots and circles). The middle top row shows spherulite formation from both random and garnet particles for the case of a sub-optimum %wt of Bi-doped LLZO. The bottom panel depicts the case where the %wt is an optimum value favoring the formation of interconnected high conductivity amorphous channels (see text for explanation).

To provide further experimental support for the role of the polymer morphology on transport in these PCEs, in the absence at this stage of our research of additional structural characterization of

the polymer morphology and spherulite formation (this is the subject of a future publication from our group), we investigated the dependence of ionic transport in PCE in membrane of different thicknesses. The central idea in this comparison is that changes in membrane thickness or when two membranes are bonded together, transport is modified as the interconnectivity of the amorphous channels is modified by structural effects.

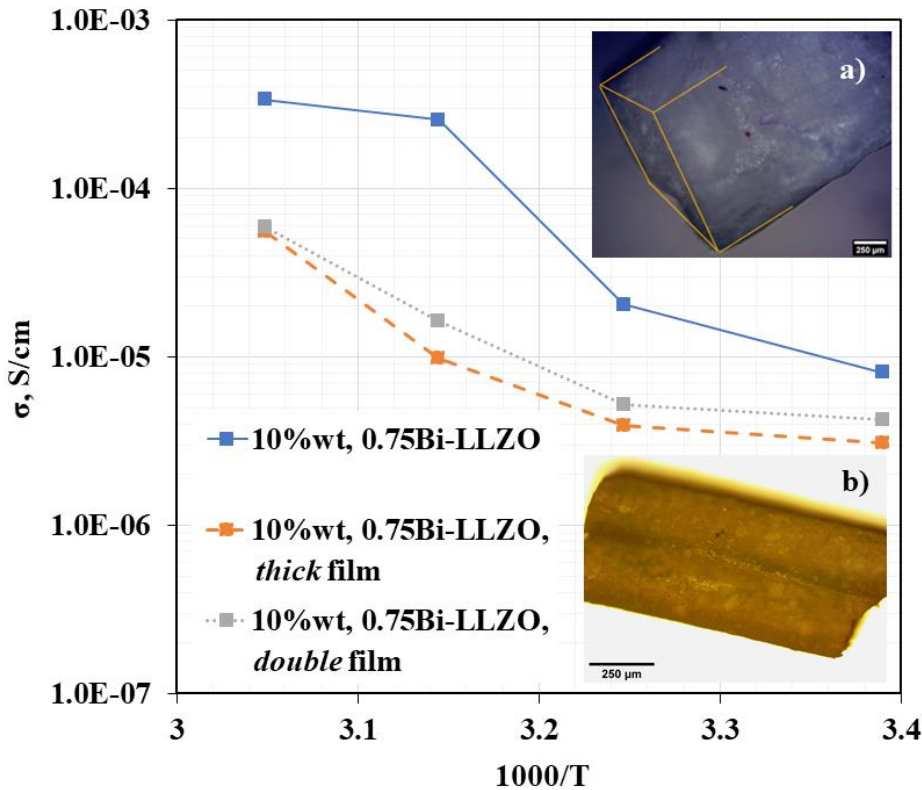


Figure 7. Ionic conductivity vs. temperature for PCE films loaded with 10%wt 0.75Bi-LLZO for membranes of different thicknesses. The plot labelled as *thin* corresponds to a $\sim 310\mu\text{m}$, *thick* refers to a $\sim 910\mu\text{m}$ sample and *double film* is made up of two separate membranes bonded by annealing two membranes, the total thickness of this sample is $\sim 500\mu\text{m}$. Inset images correspond to a) thick film and b) double film. Lines in inset a) have been added for clarity.

The nominal membrane thickness employed in this work is $\sim 310\mu\text{m}$ and the average spherulite size as reported in Fig. 5 for the 0.75Bi-LLZO at the optimum %wt of 10% is $\sim 120\mu\text{m}$. If we assume a spherical spherulite shape, this implies that at most in the direction of ion transport in the EIS measurements, there is a maximum of 3 interconnected spherulites. This implies that incrementing the membrane thickness and if the average spherulite size remains constant, a larger number of spherulites will be formed, incrementing the number of interconnections with a potential negative effect on transport. By the same reasoning, if two membranes of the same thickness are bonded together, the likelihood of joining high conductivity amorphous regions is unlikely and therefore the IC should also decrease. This is precisely what it is found and the results are illustrated in Fig. 7. In this, the ionic conductivity as a function of temperature for PCE membranes loaded with 10%wt 0.75Bi-LLZO particles is given. The highest IC across the temperature range studied is found for the $\sim 310\mu\text{m}$ membrane. The thicker membrane ($\sim 910\mu\text{m}$) and the bonded dual layers ($\sim 500\mu\text{m}$ thick) exhibit lower ionic conductivity. An important corollary of this experiment is that thinner membranes should significantly enhance the PCE ionic conductivity. Early results (to be published) from our work support this conclusion.

CONCLUSIONS

In this work, the effect of adding Bi-doped LLZO particles to PEO:LiTFSI polymer matrixes to form **Polymer Composite Electrolytes (PCE)** was investigated. The addition of garnet particles increased the ionic conductivity of the PEO:LiTFSI matrixes by factors ranging from $\sim 10x$ to $\sim 60x$ across the temperature range studied ($\sim 22^\circ\text{C}$ - $\sim 60^\circ\text{C}$). In particular, 5%wt additions of Bi-LLZO particles, resulted in IC increments of $\sim 60x$ at 35°C . The enhancement in ionic conductivity is ascribed to the formation of a PCE microstructure comprising a network of interconnected

spherulites having an optimum size and density. A plausible model to explain the observed effects was proposed. Bi-aliovalent substitution at the Zr-site in LLZO changes the Li molar ratio from Li=7.0 in LLZO to Li=6 and Li=6.25 in Bi-LLZO and 0.75Bi-LLZO garnets respectively, thereby altering the density of Li vacancies. Changes in the Li-vacancy density is suggested to modify the surface charge and chemistry of the filler particles. Said surface particle modifications impact both the Li-salt disassociation reaction and the formation and growth of spherulites in the polymer matrix nucleated at these heterogeneous sites. Changes in particle surface properties determine the weight load needed to form the optimum polymer morphology to facilitate macroscopic ion transport in the PCE.

For low weight load values, the spacing and polymer volume between filler particles is large, therefore, spherulites nucleated from both random and filler particles compete for volume, resulting in a low density of interconnected spherulites nucleated at the particle centers. For the optimal weight load, the spherulite growth nucleated by the garnet particles is dominant and it leads to the formation of large, interconnected spherulites resulting in optimal ionic conductivity. Further increase in filler particle weight load, while incrementing the number of spherulites formed, results in a decrease in spherulite size due to volume competition. In addition, the number of spherulite domain boundaries is incremented resulting in increased ion transport ohmic resistance and path tortuosity, with an overall deleterious effect on the PCE ionic conductivity. The importance of the polymer morphology and the amorphous regions interconnectivity on ionic transport is further supported by the results pertaining the IC dependence on PCE film thickness. Thick and double layer films increment spherulite interfacial resistance and the tortuosity for ion transport, negatively impacting IC.

In summary, the results presented in this work provide evidence on the critical role played by the polymer morphology of PCEs on ionic conductivity. Furthermore, we find that the Li vacancy density in the garnet particle controls the formation of the desired polymer microstructure to facilitate ion transport. *Chemical manipulation of the polymer morphology* in hybrid composite polymer electrolytes presents an attractive approach to enhance IC in this class of promising solid-state electrolytes. This study opens the possibility to further enhance ion transport in PCE through chemical manipulation and additional enhancements derived from exploring additional materials modifications. These include, the polymer molecular weight and its chemistry, the nature of the salt and of the EO:Li ratio, the garnet stoichiometry and the effect of different aliovalent dopants as well as drastically reducing the membrane thickness. On the practical side, the approach here demonstrated, can potentially decrease the fabrication costs of solid-state electrolytes while merging the best attributes of polymers and ceramic materials. We also note, that further studies are needed to provide a more comprehensive mechanistic understanding of ionic transport in these polymer composite electrolytes.

ASSOCIATED CONTENT

Supplemental information

AUTHOR INFORMATION

Corresponding Author

***E-mail: eemarinero@purdue.edu.**

Funding Sources

This research was funded in part by Dr. Marinero's startup funds from Purdue University School of Materials Engineering and in part by the Consejo Nacional de Ciencia y Tecnologia, Mexico. (CONACYT).

ACKNOWLEDGMENTS

It is a pleasure to acknowledge the following undergraduate students at Purdue University for their help with some aspects of the experimental work and measurements: David Starr, Andy Reynolds and Mai Tai. Fruitful discussions with Professors David Bahr and Jeffrey Youngblood at Purdue are also acknowledged.

REFERENCES

- (1) Liu, K.; Liu, Y.; Lin, D.; Pei, A.; Cui, Y. Materials for Lithium-Ion Battery Safety. *Science Advances*. **2018**. <https://doi.org/10.1126/sciadv.aas9820>.
- (2) Manuel Stephan, A.; Nahm, K. S. Review on Composite Polymer Electrolytes for Lithium Batteries. *Polymer*. **2006**. <https://doi.org/10.1016/j.polymer.2006.05.069>.
- (3) Agrawal, R. C.; Pandey, G. P. Solid Polymer Electrolytes: Materials Designing and All-Solid-State Battery Applications: An Overview. *J. Phys. D. Appl. Phys.* **2008**. <https://doi.org/10.1088/0022-3727/41/22/223001>.
- (4) Liao, Y. H.; Li, X. P.; Fu, C. H.; Xu, R.; Zhou, L.; Tan, C. L.; Hu, S. J.; Li, W. S. Polypropylene-Supported and Nano-Al₂O₃ Doped Poly(Ethylene Oxide)-Poly(Vinylidene Fluoride-Hexafluoropropylene)-Based Gel Electrolyte for Lithium Ion Batteries. *J. Power Sources* **2011**. <https://doi.org/10.1016/j.jpowsour.2010.10.062>.
- (5) Kumar, B.; Rodrigues, S. J.; Scanlon, L. G. Ionic Conductivity of Polymer-Ceramic Composites. *J. Electrochem. Soc.* **2001**. <https://doi.org/10.1149/1.1403729>.
- (6) Langer, F.; Bardenhagen, I.; Glenneberg, J.; Kun, R. Microstructure and Temperature Dependent Lithium Ion Transport of Ceramic-Polymer Composite Electrolyte for Solid-State Lithium Ion Batteries Based on Garnet-Type Li₇La₃Zr₂O₁₂. *Solid State Ionics* **2016**. <https://doi.org/10.1016/j.ssi.2016.04.014>.

- (7) Choi, J. H.; Lee, C. H.; Yu, J. H.; Doh, C. H.; Lee, S. M. Enhancement of Ionic Conductivity of Composite Membranes for All-Solid-State Lithium Rechargeable Batteries Incorporating Tetragonal $\text{Li}_7\text{La}_3\text{Zr}_2\text{O}_{12}$ into a Polyethylene Oxide Matrix. *J. Power Sources* **2015**. <https://doi.org/10.1016/j.jpowsour.2014.10.078>.
- (8) Li, Z.; Huang, H. M.; Zhu, J. K.; Wu, J. F.; Yang, H.; Wei, L.; Guo, X. Ionic Conduction in Composite Polymer Electrolytes: Case of PEO:Ga-LLZO Composites. *ACS Appl. Mater. Interfaces* **2019**. <https://doi.org/10.1021/acsami.8b17279>.
- (9) Wiczcerek, W.; Stevens, J. R.; Florjańczyk, Z. Composite Polyether Based Solid Electrolytes. The Lewis Acid-Base Approach. *Solid State Ionics* **1996**. [https://doi.org/10.1016/0167-2738\(96\)00042-2](https://doi.org/10.1016/0167-2738(96)00042-2).
- (10) Fan, L.; Nan, C. W.; Li, M. Thermal, Electrical and Mechanical Properties of (PEO) $_{16}$ LiClO $_4$ Electrolytes with Modified Montmorillonites. *Chemical Physics Letters*. **2003**. [https://doi.org/10.1016/S0009-2614\(03\)00043-5](https://doi.org/10.1016/S0009-2614(03)00043-5).
- (11) Yap, Y. L.; You, A. H.; Teo, L. L.; Hanapei, H. Inorganic Filler Sizes Effect on Ionic Conductivity in Polyethylene Oxide (PEO) Composite Polymer Electrolyte. *Int. J. Electrochem. Sci.* **2013**.
- (12) Wiczcerek, W. Composite Polyether Based Solid Electrolytes. The Lewis Acid-Base Approach. *Solid State Ionics* **1996**. [https://doi.org/10.1016/0167-2738\(96\)00042-2](https://doi.org/10.1016/0167-2738(96)00042-2).
- (13) Zhu, L.; Zhu, P.; Fang, Q.; Jing, M.; Shen, X.; Yang, L. A Novel Solid PEO/LLTO-Nanowires Polymer Composite Electrolyte for Solid-State Lithium-Ion Battery. *Electrochim. Acta* **2018**. <https://doi.org/10.1016/j.electacta.2018.10.005>.
- (14) Hu, L.; Tang, Z.; Zhang, Z. New Composite Polymer Electrolyte Comprising Mesoporous Lithium Aluminate Nanosheets and PEO/LiClO $_4$. *J. Power Sources* **2007**. <https://doi.org/10.1016/j.jpowsour.2007.01.028>.
- (15) Murugan, R.; Thangadurai, V.; Weppner, W. Fast Lithium Ion Conduction in Garnet-Type Li $_7$ La $_3$ Zr $_2$ O $_12$. *Angew. Chem. Int. Ed. Engl.* **2007**. <https://doi.org/10.1002/anie.200701144>.
- (16) Dong, Z.; Xu, C.; Wu, Y.; Tang, W.; Song, S.; Yao, J.; Huang, Z.; Wen, Z.; Lu, L.; Hu, N. Dual Substitution and Spark Plasma Sintering to Improve Ionic Conductivity of Garnet Li $_7$ La $_3$ Zr $_2$ O $_12$. *Nanomaterials* **2019**. <https://doi.org/10.3390/nano9050721>.
- (17) Chen, F.; Yang, D.; Zha, W.; Zhu, B.; Zhang, Y.; Li, J.; Gu, Y.; Shen, Q.; Zhang, L.; Sadoway, D. R. Solid Polymer Electrolytes Incorporating Cubic Li $_7$ La $_3$ Zr $_2$ O $_12$ for All-Solid-State Lithium Rechargeable Batteries. *Electrochim. Acta* **2017**. <https://doi.org/10.1016/j.electacta.2017.11.164>.

- (18) Marzantowicz, M.; Krok, F.; Dygas, J. R.; Florjańczyk, Z.; Zygadło-Monikowska, E. The Influence of Phase Segregation on Properties of Semicrystalline PEO:LiTFSI Electrolytes. *Solid State Ionics* **2008**. <https://doi.org/10.1016/j.ssi.2007.11.035>.
- (19) Chiang, C. Y.; Jaipal Reddy, M.; Chu, P. P. Nano-Tube TiO₂ Composite PVdF/LiPF₆ Solid Membranes. In *Solid State Ionics*; **2004**. <https://doi.org/10.1016/j.ssi.2003.12.039>.
- (20) Masoud, E. M.; El-Bellihi, A. A.; Bayoumy, W. A.; Mousa, M. A. Effect of LiAlO₂ Nanoparticle Filler Concentration on the Electrical Properties of PEO-LiClO₄ Composite. *Mater. Res. Bull.* **2013**. <https://doi.org/10.1016/j.materresbull.2012.12.012>.
- (21) Yang, T.; Zheng, J.; Cheng, Q.; Hu, Y. Y.; Chan, C. K. Composite Polymer Electrolytes with Li₇La₃Zr₂O₁₂ Garnet-Type Nanowires as Ceramic Fillers: Mechanism of Conductivity Enhancement and Role of Doping and Morphology. *ACS Appl. Mater. Interfaces* **2017**. <https://doi.org/10.1021/acsami.7b03806>.
- (22) Li, Y.; Zhang, W.; Dou, Q.; Wong, K. W.; Ng, K. M. Li₇La₃Zr₂O₁₂ Ceramic Nanofiber-Incorporated Composite Polymer Electrolytes for Lithium Metal Batteries. *J. Mater. Chem. A* **2019**. <https://doi.org/10.1039/c8ta11449h>.
- (23) Liu, W.; Lee, S. W.; Lin, D.; Shi, F.; Wang, S.; Sendek, A. D.; Cui, Y. Enhancing Ionic Conductivity in Composite Polymer Electrolytes with Well-Aligned Ceramic Nanowires. *Nat. Energy* **2017**. <https://doi.org/10.1038/nenergy.2017.35>.
- (24) Zhai, H.; Xu, P.; Ning, M.; Cheng, Q.; Mandal, J.; Yang, Y. A Flexible Solid Composite Electrolyte with Vertically Aligned and Connected Ion-Conducting Nanoparticles for Lithium Batteries. *Nano Lett.* **2017**. <https://doi.org/10.1021/acs.nanolett.7b00715>.
- (25) Wang, X.; Zhai, H.; Qie, B.; Cheng, Q.; Li, A.; Borovilas, J.; Xu, B.; Shi, C.; Jin, T.; Liao, X.; Li, Y.; He, X.; Du, S.; Fu, Y.; Dontigny, M.; Zaghbi, K.; Yang, Y. Rechargeable Solid-State Lithium Metal Batteries with Vertically Aligned Ceramic Nanoparticle/Polymer Composite Electrolyte. *Nano Energy* **2019**. <https://doi.org/10.1016/j.nanoen.2019.03.051>.
- (26) Wan, J.; Xie, J.; Kong, X.; Liu, Z.; Liu, K.; Shi, F.; Pei, A.; Chen, H.; Chen, W.; Chen, J.; Zhang, X.; Zong, L.; Wang, J.; Chen, L. Q.; Qin, J.; Cui, Y. Ultrathin, Flexible, Solid Polymer Composite Electrolyte Enabled with Aligned Nanoporous Host for Lithium Batteries. *Nat. Nanotechnol.* **2019**. <https://doi.org/10.1038/s41565-019-0465-3>.
- (27) Fu, X.; Li, Y.; Liao, C.; Gong, W.; Yang, M.; Li, R. K. Y.; Tjong, S. C.; Lu, Z. Enhanced Electrochemical Performance of Solid PEO/LiClO₄ Electrolytes with a 3D Porous Li_{6.28}La₃Zr₂Al_{0.24}O₁₂ Network. *Compos. Sci. Technol.* **2019**. <https://doi.org/10.1016/j.compscitech.2019.107863>.

- (28) Dai, J.; Fu, K.; Gong, Y.; Song, J.; Chen, C.; Yao, Y.; Pastel, G.; Zhang, L.; Wachsman, E.; Hu, L. Flexible Solid-State Electrolyte with Aligned Nanostructures Derived from Wood. *ACS Mater. Lett.* **2019**. <https://doi.org/10.1021/acsmaterialslett.9b00189>.
- (29) Wang, X.; Zhang, Y.; Zhang, X.; Liu, T.; Lin, Y. H.; Li, L.; Shen, Y.; Nan, C. W. Lithium-Salt-Rich PEO/Li 0.3 La 0.557 TiO 3 Interpenetrating Composite Electrolyte with Three-Dimensional Ceramic Nano-Backbone for All-Solid-State Lithium-Ion Batteries. *ACS Appl. Mater. Interfaces* **2018**. <https://doi.org/10.1021/acsami.8b06658>.
- (30) Marcinek, M.; Bac, A.; Lipka, P.; Zalewska, A.; Żukowska, G.; Borkowska, R.; Wieczorek, W. Effect of Filler Surface Group on Ionic Interactions in PEG–LiClO 4 –Al 2 O 3 Composite Polyether Electrolytes . *J. Phys. Chem. B* **2002**. <https://doi.org/10.1021/jp0021493>.
- (31) Schwanz, D. K. W. Solution Based Processing of Garnet Type Oxides for Optimized Lithium-Ion Transport, Purdue University, **2016**.
- (32) Oduncu, M. R. Development of a Novel Polymer-Garnet Solid State Composite Electrolyte Incorporating Li-La-Zr-Bi-O and Polyethylene Oxide. **2016**.
- (33) Schwanz, D. K.; Villa, A.; Balasubramanian, M.; Helfrecht, B.; Marinero, E. E. Bi Aliovalent Substitution in Li₇La₃Zr₂O₁₂ Garnets: Structural and Ionic Conductivity Effects. *AIP Adv.* **2020**. <https://doi.org/10.1063/1.5141764>.
- (34) Schwanz, D. K.; Marinero-Caceres, E. E. Solid-State Electrolytes and Batteries Made Therefrom, and Methods of Making Solid-State Electrolytes. 20160133990, May 12, **2019**.
- (35) Wagner, R.; Rettenwander, D.; Redhammer, G. J.; Tippelt, G.; Sabathi, G.; Musso, M. E.; Stanje, B.; Wilkening, M.; Suard, E.; Amthauer, G. Synthesis, Crystal Structure, and Stability of Cubic Li₇-XLa₃Zr₂-XBixO₁₂. *Inorg. Chem.* **2016**. <https://doi.org/10.1021/acs.inorgchem.6b01825>.
- (36) Wang, M.; Sakamoto, J. Dramatic Reduction in the Densification Temperature of Garnet-Type Solid Electrolytes. *Ionics (Kiel)*. **2018**. <https://doi.org/10.1007/s11581-018-2464-z>.
- (37) El-Shinawi, H.; Paterson, G. W.; MacLaren, D. A.; Cussen, E. J.; Corr, S. A. Low-Temperature Densification of Al-Doped Li₇La₃Zr₂O₁₂: A Reliable and Controllable Synthesis of Fast-Ion Conducting Garnets. *J. Mater. Chem. A* **2017**. <https://doi.org/10.1039/c6ta06961d>.
- (38) Li, L.; Feng, L.; Zhang, Y.; Peng, H.; Zou, Y. Low Temperature, Fast Synthesis and Ionic Conductivity of Li₆MLa₂Nb₂O₁₂ (M = Ca, Sr, Ba) Garnets. *J. Sol-Gel Sci. Technol.* **2017**. <https://doi.org/10.1007/s10971-017-4453-5>.

- (39) Lascaud, S.; Perrier, M.; Vallée, A.; Besner, S.; Prud'homme, J.; Armand, M. Phase Diagrams and Conductivity Behavior of Poly(Ethylene Oxide)-Molten Salt Rubbery Electrolytes. *Macromolecules* **1994**. <https://doi.org/10.1021/ma00103a034>.
- (40) Shin, J. H.; Lim, Y. T.; Kim, K. W.; Ahn, H. J.; Ahn, J. H. Effect of Ball Milling on Structural and Electrochemical Properties of (PEO)NLiX (LiX = LiCF₃SO₃ and LiBF₄) Polymer Electrolytes. *J. Power Sources* **2002**. [https://doi.org/10.1016/S0378-7753\(01\)00990-9](https://doi.org/10.1016/S0378-7753(01)00990-9).
- (41) Devaux, D.; Bouchet, R.; Glé, D.; Denoyel, R. Mechanism of Ion Transport in PEO/LiTFSI Complexes: Effect of Temperature, Molecular Weight and End Groups. *Solid State Ionics* **2012**. <https://doi.org/10.1016/j.ssi.2012.09.020>.
- (42) Paoella, Andrea; Zhu, Wen; Bertoni, Giovanni; Savoie, Sylvio; Feng, Zimin; Demers, Hendrix; Gariepy, Vincent; Girard, Gabriel; Rivard, Etienne; Delaporte, Nicolas; Guerfi, Abdelbast; Lorrmann, Henning; George, Chandramohan; Zaghbi, Karim. Discovering the Influence of Lithium Loss on Garnet Li₇La₃Zr₂O₁₂ Electrolyte Phase Stability. *ACS Applied Energy Materials*. **2020**. <https://doi.org/10.1021/acsaem.9b02401>.
- (43) Malathi, M.; Tamilarasan, K.; Ganesan, V. Role of Ceramic Reinforcement in Composite Polymer Electrolyte. *Polym. Compos.* **2015**. <https://doi.org/10.1002/pc.22910>.
- (44) Mohamed Ali, T.; Padmanathan, N.; Selladurai, S. Effect of Nanofiller CeO₂ on Structural, Conductivity, and Dielectric Behaviors of Plasticized Blend Nanocomposite Polymer Electrolyte. *Ionics (Kiel)*. **2015**. <https://doi.org/10.1007/s11581-014-1240-y>.
- (45) Marzantowicz, M.; Dygas, J. R.; Krok, F.; Łasińska, A.; Florjańczyk, Z.; Zygadło-Monikowska, E.; Affek, A. Crystallization and Melting of PEO:LiTFSI Polymer Electrolytes Investigated Simultaneously by Impedance Spectroscopy and Polarizing Microscopy. In *Electrochimica Acta*; **2005**. <https://doi.org/10.1016/j.electacta.2005.02.053>.
- (46) Chen, L.; Li, Y.; Li, S. P.; Fan, L. Z.; Nan, C. W.; Goodenough, J. B. PEO/Garnet Composite Electrolytes for Solid-State Lithium Batteries: From “Ceramic-in-Polymer” to “Polymer-in-Ceramic.” *Nano Energy* **2018**. <https://doi.org/10.1016/j.nanoen.2017.12.037>.
- (47) Xi, J.; Tang, X. Investigations on the Enhancement Mechanism of Inorganic Filler on Ionic Conductivity of PEO-Based Composite Polymer Electrolyte: The Case of Molecular Sieves. *Electrochim. Acta* **2006**. <https://doi.org/10.1016/j.electacta.2006.01.016>.
- (48) Xi, J.; Qiu, X.; Wang, J.; Bai, Y.; Zhu, W.; Chen, L. Effect of Molecular Sieves ZSM-5 on the Crystallization Behavior of PEO-Based Composite Polymer Electrolyte. *J. Power Sources* **2006**. <https://doi.org/10.1016/j.jpowsour.2005.10.010>.

- (49) Croce, F.; Settini, L.; Scrosati, B. Superacid ZrO₂-Added, Composite Polymer Electrolytes with Improved Transport Properties. *Electrochem. commun.* **2006**. <https://doi.org/10.1016/j.elecom.2005.12.002>.
- (50) Tominaga, Y.; Endo, M. Ion-Conductive Properties of Polyether-Based Composite Electrolytes Filled with Mesoporous Silica, Alumina and Titania. *Electrochim. Acta* **2013**. <https://doi.org/10.1016/j.electacta.2013.09.117>.
- (51) Cheng, S.; Smith, D. M.; Li, C. Y. How Does Nanoscale Crystalline Structure Affect Ion Transport in Solid Polymer Electrolytes? *Macromolecules* **2014**. <https://doi.org/10.1021/ma500734q>.
- (52) Fullerton-Shirey, S. K.; Maranas, J. K. Effect of LiClO₄ on the Structure and Mobility of PEO-Based Solid Polymer Electrolytes. *Macromolecules* **2009**. <https://doi.org/10.1021/ma802502u>.
- (53) Homminga, D.; Goderis, B.; Dolbnya, I.; Reynaers, H.; Groeninckx, G. Crystallization Behavior of Polymer/Montmorillonite Nanocomposites. Part I. Intercalated Poly(Ethylene Oxide)/Montmorillonite Nanocomposites. *Polymer (Guildf)*. **2005**. <https://doi.org/10.1016/j.polymer.2005.10.016>.
- (54) Huang, Z.; Wang, S.; Kota, S.; Pan, Q.; Barsoum, M. W.; Li, C. Y. Structure and Crystallization Behavior of Poly(Ethylene Oxide)/Ti₃C₂T_x MXene Nanocomposites. *Polymer (Guildf)*. **2016**. <https://doi.org/10.1016/j.polymer.2016.09.011>.
- (55) Fullerton-Shirey, S. K.; Maranas, J. K. Structure and Mobility of PEO/LiClO₄ Solid Polymer Electrolytes Filled with Al₂O₃ Nanoparticles. *J. Phys. Chem. C* **2010**. <https://doi.org/10.1021/jp906608p>.

Optimizing Ionic Transport in Polymer (PEO) – Garnet (LLZO) Composite Solid-State Electrolytes

*Andres Villa, Juan Carlos Verduzco and Ernesto E. Marinero**

***School of Materials Engineering, Purdue University, Neil Armstrong Hall of Engineering,
701 West Stadium Avenue, West Lafayette, IN 47907.**

SUPPLEMENTAL INFORMATION

This section provides additional information on sample synthesis, measurements and details on the derivation of parameters reported in the main text. To decrease the average Bi-LLZO and 0.75Bi-LLZO particle size, the garnet powders were mixed with polyethylene oxide (PEO, Sigma Aldrich, molecular weight 100,000), lithium bis(trifluoromethanesulfonyl)imide (LiTFSI, Sigma Aldrich, 99.8%) and acetonitrile (ACN, Sigma Aldrich, 99.9%) was used as the solvent to fully mix the composite materials. ACN was mixed at a 2.5:1 liquid to solids ratio to form a PCE slurry. All the materials were ball milled for 12 hours at 400 rpm with a Fritsch Pulverisette 6 apparatus. Milling for 12 hours at 400 rpm yielded mesoparticles of ~437nm (d_{50}) in size. High purity 100 x 42 x 18 mm yttrium stabilized zirconia boats were obtained from MTI Corporation for high temperature calcination of ceramic precursors. A 100 ml yttrium stabilized zirconium oxide jar with lid and yttrium stabilized zirconium oxide spherical grinding media (5 mm in diameter) were purchased from Across International for ball milling experiments.

The choice for the milling time and rpm was based on our studies¹ of the dependence of particle size on wet-ball milling process parameters. Fig. S1 presents SEM images of powders milled at 400 rpm for 1h, 2h, 6h and 8h. The average particle size was observed to decrease from ~ 1 μ m to ~ 680nm. Increasing the milling time to 12h resulted in an average particle size of ~ 430nm and a significant reduction of large particles. ImageJ software² was used to determine the average particle size of the LLZO powder from SEM images. ImageJ calculates area and pixel value statistics of user-defined selections and intensity-thresholded objects. It can create density histograms and line profile plots. An example of a histogram obtained after 8h of milling time is shown in Fig. S2. The orange curve shows the cumulative percent and is used to determine d_{50} .

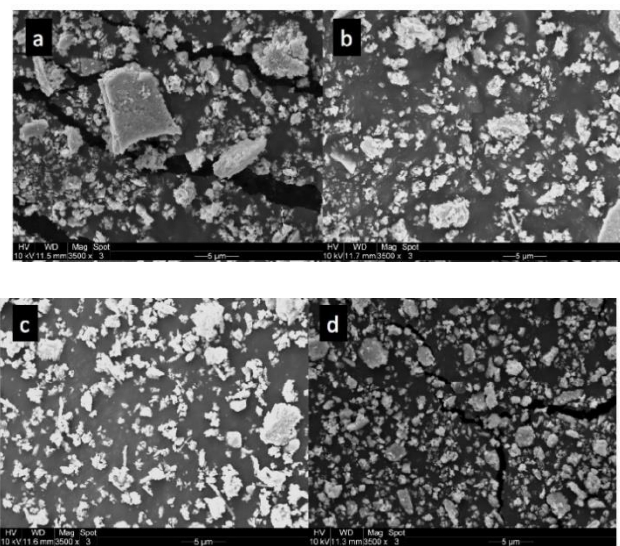


Figure S1. SEM images of ball-milled LLZBO particles as a function of milling time: a) 1h, b) 2h, c) 4h and d) 8 h. Significant particle size reduction is observed for long milling times. The average particle sizes was estimated from ImageJ analysis to decrease from ~1 μ m, to ~ 680nm.

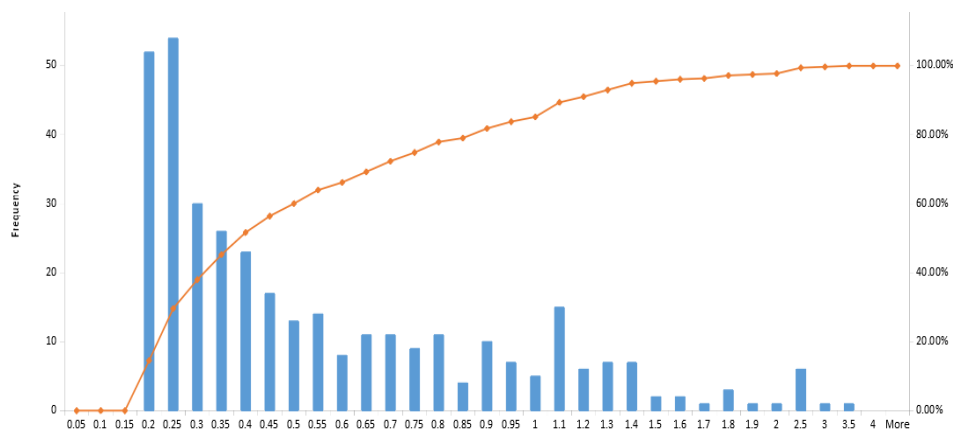


Figure S2. Particle size distribution for Bi-LLZO particles after 8h of ball-milling at 400 rpm. The orange curve shows the cumulative undersize % where d_{50} is ~ 400 nm.

To obtain a distribution of garnet particles homogeneously embedded in the film, the resulting slurry after ball-milling was deposited in a flexible mold and the solvent was allowed to evaporate slowly over 72h at room temperature and atmospheric pressure, with an additional 24h under vacuum and room temperature. Fig. S3 presents SEM images of PEO:LiTFSI polymer matrixes loaded with Bi-LLZO particles. Fig. S3(a) corresponds to 5%wt and it shows a rather uniform distribution of Bi-LLZO particles within a contiguous, smooth polymer surface. Note the large separation of the garnet particles and as described in the main text, this particle load yielded the highest IC in this PCE. Loading the polymer matrix with Bi-LLZO 50%wt, Fig. S3(b) resulted in a rougher surface, exhibiting cracks in the middle of the image. We note that these images are representative of the particle distribution at the surface of the $\sim 500\mu\text{m}$ thick films examined.

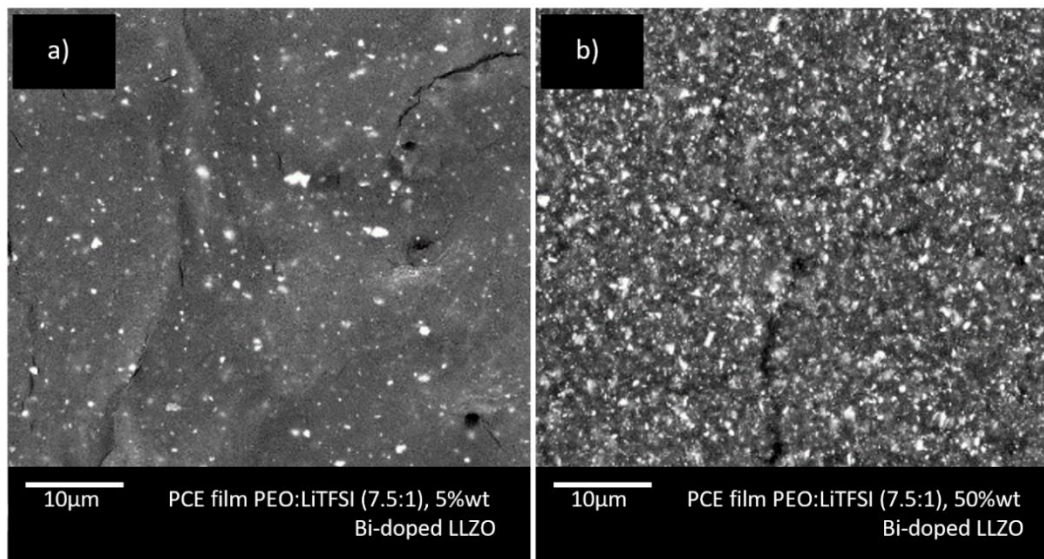


Figure S3. SEM images of LLZBO particles dispersed in PEO. The weight load in (a) is 5%, whereas that for (b) 50%. A relative uniform dispersion of particles is observed, however, the high load leads to formation of cracks in the polymer matrix.

Melting temperature of PCE films was determined through DSC curve analysis using TA Instruments Q2000 equipment. Sample films were sealed in Al pans, scanned to 100°C, then to -100°C, and finally to 100°C, at a rate of 20°/min. Figure S4 shows DSC scans for PEO:LiTFSI films with Bi-LLZO, as well as an unloaded sample, and another with 5% wt Al₂O₃ to compare the effect of a passive filler. The heat flow is normalized to the mass of PEO.

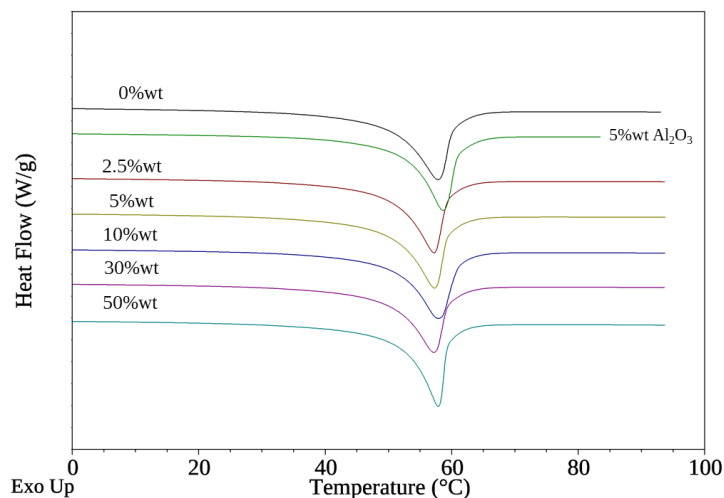


Figure S4. DSC scans for films PEO:LiTFSI with added % wt of Bi-LLZO as well added % wt of Al_2O_3 . Scans are shifted vertically for clarity.

Table S1. Values of ΔH_m and T_m obtained from DSC for films with Bi-LLZO and Al_2O_3 .

	ΔH_m	T_m
0%	107	57.9
5% Al_2O_3	106	58.6
2.5	103	57.2
5	104	57.3
10	103	57.9
30	98.7	57.2
50	104	57.9

To investigate the effect of film thickness on the IC of PCEs, three types of films were prepared. “Thin” films (thickness between 250 and 310 μm) were cast on a 1” x 1” square-shaped mold, 1 mm deep mold using a syringe to pour the slurry. To prepare “thick” films ($\sim 910\mu\text{m}$), the PCE slurry was poured with a syringe into a similar square-shaped casting mold (with a 2mm thickness

and a 5mm by 5 mm area). Finally, to prepare the thin “double” films (~500 μ m), sample “thin” films were dabbed with a q-tip with acetonitrile (ACN) and were sandwiched. Optical microscopy was used to characterize the thickness of the “thick” films and thin “double” films.

To study spherulites utilizing polarized light microscopy, the following procedure was utilized to obtain suitable samples for analysis. Films were prepared using the same procedure used to perform electrochemical impedance spectroscopy (EIS) characterization. The samples were then loaded onto the sample fabrication mold and heated to 99°C while pressing on them with a glass slide for 10 minutes using a 200g weight, the purpose of this annealing and pressing procedure was to decrease the sample thickness to facilitate light transmission through the sample (the samples as prepared were prohibitively thick). Upon cooling to room temperature, the top glass slide was removed and the decreased-thickness film was placed on the casting mold for PLM observations. First, the microscope heating stage temperature was increased to 99°C and the polymer was then cooled down from the melt at a rate of 5°C/min, and held at 35°C. We note that observations were only made in the 5%wt and 10%wt garnet loaded samples, as at higher particle load yielded samples that were not translucent enough to acquire high quality images due to garnet particle absorption and scattering.

This methodology to prepare samples for PLM that involves heating the polymer above its melting point while subjecting it to a load to decrease their thickness to make them optically transparent specimens and subsequently cooling them down to the desired observation temperature desired has been successfully utilized in studies of spherulite formation in PEO:LiTFSI thin films^{3,4}. Although the thermal history of samples characterized by PLM in our work differs from those measured by EIS, the experimental procedure used to prepare all PLM was identical. This argues in favor that the trends observed regarding the spherulite growth as a function of particle

wt load is basis are valid. However, we recognize that the kinetics of spherulite nucleation and growth is influenced by the thermal history of the sample and therefore the spherulite dimensions reported in this work likely would differ, were the samples not first exposed to 99°C.

Calculations for the IC were conducted using electrochemical impedance spectroscopy (EIS) and measurements were analyzed and fit using an RC model with both a resistive and capacitive component in parallel, where the magnitude of the real component of the semi-circle observed, for example in figure S5 at 23°C, represent the resistive element, R. Using the measured thickness and area of the sample, equation S1 can be used to determine the IC. (S1)

$$\sigma = \frac{t}{AR}$$

As the measurement temperature is increased, the semi-circle decreased in magnitude, and started to disappear at 45°C and 55°C, indicating increasing capacitive behavior and decreasing resistance for ionic conduction.

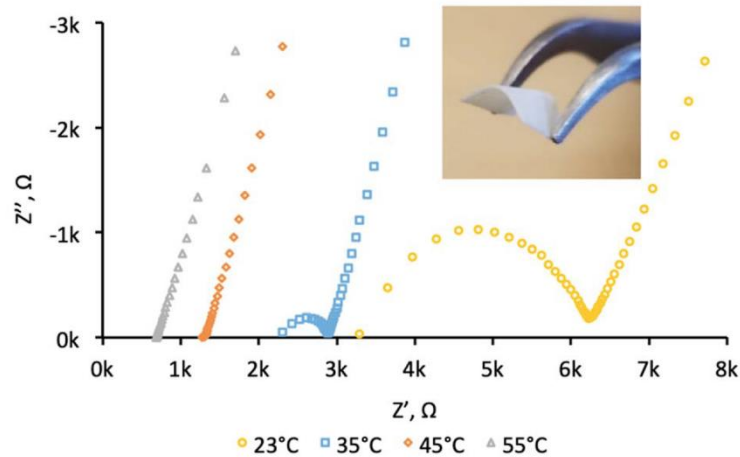


Figure S5. Nyquist plots for Bi-LLZO polymer composite electrolyte films at 23°C, 35°C, 45°C and 55°C. Inset is an image of tweezers holding a sample film of 5% wt Bi-LLZO film.

To understand the effect of %wt load on ionic conductivity, Arrhenius analysis of the data presented in Fig. 2 was conducted with an objective to identify variations in activation energy for transport. To first order, we assume that the transport mechanism is an activated diffusion process that has an Arrhenius relationship with temperature, wherein ion motion across the polymer structure is hindered by microscopic processes that can be represented by an activation energy that must be surmounted for efficient ion transport. Below the PEO melting point we assume that the activated process can be to first order described by Eq. S2 and the activation energy E_A can be derived from a logarithm plot of the ionic conductivity (σ) vs the inverse temperature ($1/T$). Also, the Boltzmann constant is k_B and A is a pre-exponential factor. (S2)

$$\sigma = Ae^{-\left(\frac{E_a}{2.3k_B T}\right)}$$

Fig. S6 presents the Arrhenius analysis of IC for polymer matrixes loaded with 0.75 Bi-LLZO and Bi-LLZO particles. The line slopes were calculated using a linear fit. A similar approach to estimate activation energy for transport in PCE is reported by Choi *et al.*⁵ for the case of PEO loaded with tetragonal LLZO. In Table S2 the values of the activation energies derived from the analysis are presented.

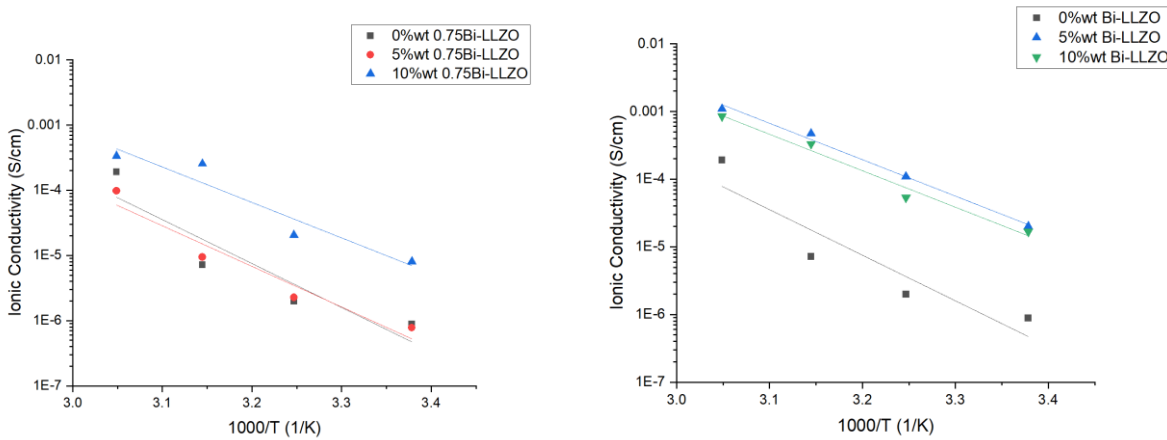


Figure S6. Arrhenius analysis and activation energy derivation for PCE samples with 0%wt, 5%wt and 10%wt of 0.75 Bi-LLZO and Bi-LLZO filler particles added to the polymer matrix.

Table S2. Activation energies for PEO:LiTFSI films loaded with Bi-LLZO and 0.75Bi-LLZO.

wt%	0.75Bi-LLZO	Bi-LLZO
	E_A (eV)	E_A (eV)
0%	1.34	1.34
5%	1.24	1.07
10%	1.08	1.07
30%	1.2	1.2
50%	0.69	1.22

A clear decrease of the activation energy for ion transport can be observed at the %wt resulting in optimum IC for the 0.75Bi-LLZO (10%) and Bi-LLZO (5-10%) consistent with results reported in this work. XRD was used to determine the phase purity of the calcined powders before ball-milling. MAUD was used to perform Rietveld refinement of the data⁶. To determine the phase of $\text{La}_2\text{Zr}_2\text{O}_7$ ⁷ in the calcined powders, the reference CIS file reported by Hamao⁸ was employed and the appropriate substitution of Bi atoms at known Li and Zr sites⁹. The Li1 and Li2 site occupation information based on published work¹⁰⁻¹² was also employed. Figure S7 shows the fitting for Rietveld refinement for Bi-LLZO and 0.75Bi-LLZO. For the case of Bi-LLZO the crystalline $\text{La}_2\text{Zr}_2\text{O}_7$ phase was estimated at ~2.08%wt, while for the 0.75Bi-LLZO powders it is estimated at ~1.03%wt. These calculations were in agreement and in similar values to those reported previously, where a value of ~3%wt was reported¹³.

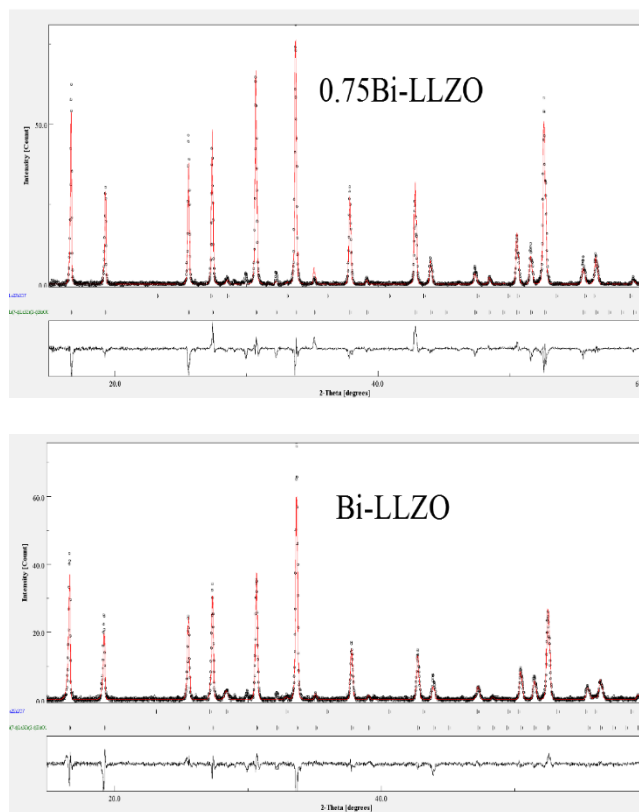


Figure S7. Observed (black), calculated (red) and difference patterns (below observed and calculated patterns) for XRD patterns of Bi-LLZO and 0.75Bi-LLZO garnets. The short peak at 28.45° represents presence of $L_2Zr_2O_7$.

SUPPLEMENTAL REFERENCES

- (1) Oduncu, M. R. Development of a Novel Polymer-Garnet Solid State Composite Electrolyte Incorporating Li-La-Zr-Bi-O and Polyethylene Oxide. **2016**.
- (2) Schneider, C. A.; Rasband, W. S.; Eliceiri, K. W. NIH Image to ImageJ: 25 Years of Image Analysis. *Nature Methods*. 2012. <https://doi.org/10.1038/nmeth.2089>.
- (3) Marzantowicz, M.; Dygas, J. R.; Krok, F.; Nowiński, J. L.; Tomaszewska, A.; Florjańczyk, Z.; Zygadło-Monikowska, E. Crystalline Phases, Morphology and Conductivity of PEO:LiTFSI Electrolytes in the Eutectic Region. *J. Power Sources* **2006**. <https://doi.org/10.1016/j.jpowsour.2006.02.044>.
- (4) Zhang, X.; Zhou, L.; Wang, Y.; Zhou, Q. Influence of Humidity on the Complex Structure of PEO-Lithium Salt Polymer Electrolyte. *Polym. Sci. - Ser. A* **2018**. <https://doi.org/10.1134/S0965545X18010091>.
- (5) Choi, J. H.; Lee, C. H.; Yu, J. H.; Doh, C. H.; Lee, S. M. Enhancement of Ionic Conductivity of Composite Membranes for All-Solid-State Lithium Rechargeable Batteries Incorporating Tetragonal Li₇La₃Zr₂O₁₂ into a Polyethylene Oxide Matrix. *J. Power Sources* **2015**. <https://doi.org/10.1016/j.jpowsour.2014.10.078>.
- (6) Lutterotti, L. Total Pattern Fitting for the Combined Size-Strain-Stress-Texture Determination in Thin Film Diffraction. *Nucl. Instruments Methods Phys. Res. Sect. B Beam Interact. with Mater. Atoms* **2010**. <https://doi.org/10.1016/j.nimb.2009.09.053>.
- (7) Hagiwara, T.; Nomura, K.; Kageyama, H. Crystal Structure Analysis of Ln₂Zr₂O₇ (Ln = Eu and La) with a Pyrochlore Composition by High-Temperature Powder X-Ray Diffraction. *J. Ceram. Soc. Japan* **2017**. <https://doi.org/10.2109/jcersj2.16248>.
- (8) Hamao, N.; Kataoka, K.; Kijima, N.; Akimoto, J. Synthesis, Crystal Structure and Conductive Properties of Garnet-Type Lithium Ion Conductor Al-Free Li_{7-x}La₃Zr₂-XTaxO₁₂ (0 ≤ x ≤ 0.6). *J. Ceram. Soc. Japan* **2016**. <https://doi.org/10.2109/jcersj2.16019>.
- (9) Schwanz, D. K.; Villa, A.; Balasubramanian, M.; Helfrecht, B.; Marinero, E. E. Bi Aliovalent Substitution in Li₇La₃Zr₂O₁₂ Garnets: Structural and Ionic Conductivity Effects. *AIP Adv.* **2020**. <https://doi.org/10.1063/1.5141764>.
- (10) Meier, K.; Laino, T.; Curioni, A. Solid-State Electrolytes: Revealing the Mechanisms of Li-Ion Conduction in Tetragonal and Cubic LLZO by First-Principles Calculations. *J. Phys. Chem. C* **2014**. <https://doi.org/10.1021/jp5002463>.

- (11) Xiang, X.; Liu, Y.; Chen, F.; Yang, W.; Yang, J.; Ma, X.; Chen, D.; Su, K.; Shen, Q.; Zhang, L. Crystal Structure and Lithium Ionic Transport Behavior of Li Site Doped $\text{Li}_7\text{La}_3\text{Zr}_2\text{O}_{12}$. *J. Eur. Ceram. Soc.* **2020**. <https://doi.org/10.1016/j.jeurceramsoc.2020.02.054>.
- (12) Wagner, R.; Rettenwander, D.; Redhammer, G. J.; Tippelt, G.; Sabathi, G.; Musso, M. E.; Stanje, B.; Wilkening, M.; Suard, E.; Amthauer, G. Synthesis, Crystal Structure, and Stability of Cubic $\text{Li}_{7-x}\text{La}_3\text{Zr}_{2-x}\text{Bi}_x\text{O}_{12}$. *Inorg. Chem.* **2016**, *55* (23), 12211–12219.
- (13) Wolfenstine, J.; Ratchford, J.; Rangasamy, E.; Sakamoto, J.; Allen, J. L. Synthesis and High Li-Ion Conductivity of Ga-Stabilized Cubic $\text{Li}_7\text{La}_3\text{Zr}_2\text{O}_{12}$. *Mater. Chem. Phys.* **2012**. <https://doi.org/10.1016/j.matchemphys.2012.03.054>.